33rd Annual International Conference of the IEEE EMBS
Boston, Massachusetts USA, August 30 - September 3, 2011

Current Steering and Current Focusing with a High-Density Intracochlear Electrode Array

Jessica D. Falcone, *Student Member, IEEE*, Pamela T. Bhatti, *Member, IEEE*

***Abstract*—Creating high-resolution or high-density, intracochlear electrode arrays may significantly improve quality of hearing for cochlear implant recipients. Through focused activation of neural populations such arrays may better exploit the cochlea's frequency-to-place mapping, thereby improving sound perception. Contemporary electrode arrays approach high-density stimulation by employing multi-polar stimulation techniques such as current steering and current focusing. In our procedure we compared an advanced high-density array with contemporary arrays employing these strategies. We examined focused stimulation of auditory neurons using an activating function and a neural firing probability model that together enable a first-order estimation of an auditory nerve fiber's response to electrical stimulation. The results revealed that simple monopolar stimulation with a high-density array is more localized than current steering with a contemporary array and requires 25-30% less current. Current focusing with high-density electrodes is more localized than current focusing with a contemporary array; however, a greater amount of current is required. This work illustrates that advanced high-density electrode arrays may provide a low-power, high-resolution alternative to current steering with contemporary cochlear arrays.**

I. Introduction

COCHLEAR implants (CIs) electrically stimulate the auditory nerve and restore functional hearing to individuals experiencing sensorineural deafness. Despite improvements in speech perception over the past decades [1], a number of CI users experience difficulty with understanding speech in noisy environments, comprehension of tonal language (i.e. Mandarin, Punjabi), and music appreciation. One solution to improving on these deficiencies is to increase the resolution, or number of electrodes, on the CI array. However, size restrictions due to current electrode manufacturing techniques and physical dimensions of the cochlea prevent this number from increasing.

To compensate for the lack of high resolution, techniques such as current steering (CS) and current focusing (CF) were developed. CS stimulates the neural populations between the electrodes and CF more selectively stimulates the target neural populations [1],[2]. An alternative approach to increasing resolution incorporates micro-electromechanical systems fabrication methods to create a thin film microelectrode array with a series of high-density electrodes [3],[4]. When combined with advanced signal-processing algorithms, a high-density electrode array such as this may be pivotal to improving hearing for CI users. In this work we compare a novel high-density array to contemporary arrays in terms of their ability to activate restricted populations of neurons as well as the associated currents required to achieve stimulation.

Manuscript received April 15, 2011. Partial support of this research was provided by the Woodrow W. Everett, Jr. SCEEE Development Fund in cooperation with the Southeastern Association of Electrical and Computer Engineering Department Heads.

J. Falcone and P. Bhatti are with the School of Electrical and Computer Engineering at the Georgia Institute of Technology, Atlanta GA 30332-0250 USA. (phone: 404-385-3144; fax: 404-894-8750; e-mail: pamela.bhatti@ece.gatech.edu).

II. Background

Four CI companies compete in today's market: Advanced Bionics, Cochlear, Med-El, and MxM Neurelec. When comparing the devices offered by each company, the total number of electrodes ranges from 12 to 22, the electrode diameters vary from 0.5 to 1.3 mm, and the midpoint electrode spacing ranges from 0.85 to 2.4 mm [5]–[8]. All contemporary arrays are manufactured by hand. In contrast, a thin-film high-density array is batch-fabricated on a single wafer. Silicon-based arrays with electrode diameters of 0.18 mm and a midpoint electrode spacing of 0.25 mm have been fabricated achieving 1µm features [2].

Presently CI manufacturers attempt to approach high-density stimulation with existing arrays, but require the use of multiple sites in parallel using techniques including current steering and current focusing. Current steering (CS) is a phenomenon that occurs when two physical electrodes are stimulated simultaneously by a weighted current (Fig. 1a–b). The summation of the electrical fields stimulates nerves located between the two physical electrodes which are not normally activated by a single electrode. This results in CI patients hearing an intermediary pitch percept [9]. CS is measured in terms of α, which represents the weighted percentage of current on the second electrode [9-11].

Current focusing (CF) requires three electrodes, where a positive current is applied to the central electrode and a percentage of negative current is applied to the two side

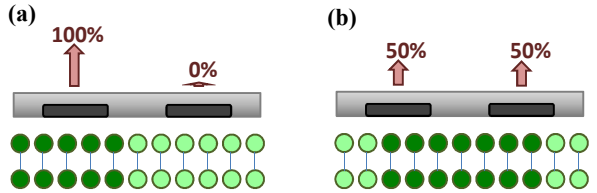

Fig. 1. For CS, (a) α = 0 when at electrode 1, *I = 100%,* and at electrode 2, *I = 0%,* and (b) α = 0.5 when at electrode 1, *I = 50%,* and at electrode 2, *I = 50%.* Stimulated neurons are darkened.

electrodes (Fig. 2a–b). The resulting summation creates a narrower field of excitation. CF is measured in terms of σ, which is the summation of the weighted percentage of current on the side electrodes [9]-[11].

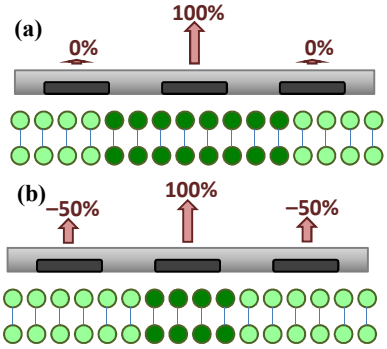

Fig. 2. For CF, at electrode 2, *I = 100%*, and (a) σ = 0 when at electrode 1 and 3, *I = 0%*, and (b) σ = 1 when at electrode 1 and 3, *I = –50%*. Stimulated neurons are darkened.

III. Methods

To simulate and compare high-density and contemporary electrodes, a first order estimation model was developed by incorporating an activating function [12] and a neural firing probability model for auditory nerve fibers [15]. In this model the electrode array is located along the *x*-axis and the auditory nerve fibers are oriented along the *z*-axis. A distance of *d*, in the *y* direction, separates the electrodes and an auditory nerve fiber cluster consisting of 100 fibers (Fig. 3). The equations are evaluated in terms of *x* to view the effects of stimulation across the different fibers.

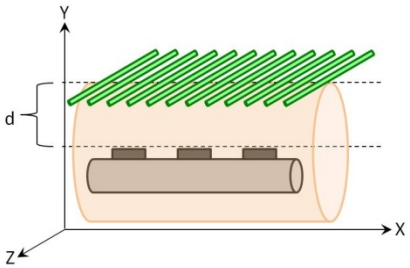

Fig. 3. Simplified model of the cochlea (orange), auditory nerve fiber clusters (green), and electrode array (light brown) with electrodes (dark brown).

A. Activating Function

The activating function (AF) represents the neural response to electrical stimulation [12]. The AF (1) is the second derivative of the external potential (2). As seen in both equations, ρ_e is the extracellular resistivity, I is the electrode current, and x, y, and z are the coordinates of the electrode relative to the nerve fiber. The derivative is taken in terms of the coordinate axis that runs parallel to the length of the fiber [12],[13]. For the simplified cochlea/auditory nerve model, the AF is derived in terms of z (the orientation of the nerve fibers). Next, y is set equal to d and z is set equal to 0, leaving x and I as the inputs for AF (3). Based on computed tomography data of inserted electrode arrays in human cadavers, we set d at a distance of 0.7 mm [4].

$$\mathrm{AF}(x,y,z,I) = \frac{\rho_e \cdot I}{4\pi} \cdot \left[\frac{-1}{(x^2+y^2+z^2)^{3/2}} + \frac{3z/2}{(x^2+y^2+z^2)^{5/2}} \right] \quad (1)$$

$$V_e(x,y,z,I) = \frac{\rho_e}{4\pi} \cdot \frac{I}{\sqrt{x^2+y^2+z^2}} \quad (2)$$

$$AF(x,I) = \frac{\rho_e \cdot I}{4\pi} \cdot \left[\frac{-1}{(x^2+d^2)^{3/2}} \right] \quad (3)$$

For CS the overall AF is the summation of the AF's of the first electrode (*assigned to location* x_1) and the second electrode (*assigned to location* x_2). The input current (I) of the first electrode is multiplied by $(1-\alpha)$ and I of the second electrode is multiplied by α [14].

$$AF_{CS} = AF_1(x_1, (1-\alpha)\cdot I) + AF_2(x_2, \alpha \cdot I) \quad (4)$$

For CF, the overall AF is the summation of the AFs of the first, second and third electrodes (x_1, x_2, and x_3). The input current (I) of the first and third electrode is multiplied by $-\sigma/2$, and I of the second electrode is not altered [15].

$$AF_{CF} = AF_1(x_1, -\sigma/2 \cdot I) + AF_2(x_2, I) + AF_3(x_3, -\sigma/2 \cdot I) \quad (5)$$

B. Neural Firing Probability Model

This model calculates the firing probability of a single nerve fiber (j) due to electrical stimulation.

$$P(x,j) = \Phi\left[\frac{|AF(x,I_{el})| - AF_{thr}(x,j)}{AF_{thr}(x,j) * RS(x,j)}\right] \quad (6)$$

The probability is calculated by subtracting the AF threshold (AF_{thr}) from the absolute value of the AF, and the resulting difference is divided by the multiple of the AF_{thr} and the relative spread (RS). Finally, the cumulative normal distribution (Φ) is taken and the probability is determined. The relative spread is a constant that relates firing probability to stimulus threshold. It is calculated by generating a random number from a normal distribution with a mean of 0.0635 and a standard deviation of 0.04. The resulting number is then clipped within the range of 0.03 and 0.1. The AF_{thr} is determined by generating a random number from a log-normal distribution, which is assumed to have a standard deviation to mean ratio of 0.3. The mean of the AF_{thr} is arbitrarily set to 0 dB. This arbitrary assignment is inconsequential when comparing the relative neural activity levels [15]. To calculate the firing response of the auditory nerve fiber, a uniformly distributed random variable (RV) is generated from [0, 1]. The $P(x, j)$ of the individual fiber is compared to RV. If the probability is greater than or equal to RV, the auditory nerve fiber fires (N). For each neural cluster of 100 fibers at x, all fired auditory nerve fibers are summed (ΣN) [15]. The assumption was made that ΣN equaled the loudness heard by the CI patient [15]. Therefore, the different stimulation scenarios were compared relatively via summed number of auditory nerve fibers fired (ΣN) at levels of 250, 500, and 1000.

C. Greenwood Function

The Greenwood function was used to map the frequency-to-position relation of the cochlea [17].

$$f(x) = A(10^{a(x-31)} - K) \quad (7)$$

The frequency (*f*) is calculated in terms of distance along the cochlea (*x*). The apex of the cochlea is at $x = 0$. Based on the measurements for humans, the frequency scaling constant *(A)* is 165.4 Hz, the frequency integration constant *(K)* is 0.88 Hz, and the frequency-position slope (*a)* is 0.06. The equation was modified to set the base of the cochlea to $x = 0$ with the total length of the cochlea set to 31 mm [18]. Thus the *x* variable in the activating function and the following neural firing probability model was converted into frequency [19].

IV. Results

Two different stimulation comparisons were evaluated: CS in a conventional electrode array vs. normal stimulation in a high-density array, and CF with a contemporary array vs. CF in a high-density array. For the first scenario, a contemporary array was modeled with two stimulating sites located at 9.5 mm and 10.5 mm along the x-axis giving a 1 mm separation distance. These two electrodes underwent CS with $\alpha = 0.5$, which ideally would have stimulated the neural population maximally around 10 mm (equidistance between the two electrodes). This neural response was then compared to that of monopolar stimulation with a high-density array incorporating a single electrode located at 10 mm. As shown in Fig. 4a-c, CS and the high-density electrode were evaluated in terms of summed total of neurons fired ($\Sigma N = 250, \Sigma N = 500, \Sigma N = 1000$). With each ΣN, the high-density electrode produced a more localized stimulation then its CS counterpart. Next, CF with $\sigma = 1$ was compared between three contemporary and three high-density array electrodes. The contemporary sites were located at 9 mm, 10 mm, and 11 mm, with an end-to-end spacing of 1 mm. The high-density electrodes were located at 9.75 mm, 10 mm, and 10.25 mm, with an end-to-end spacing of 0.25 mm. As seen in Fig. 5, the contemporary and high-density electrodes were compared in terms of summed total neurons fired ($\Sigma N = 250, \Sigma N = 500, \Sigma N = 1000$). CF using high-density electrodes appeared to create a more focused neural response; however, current consumption of CF with high-density electrodes was significantly higher than CF with contemporary electrodes.

V. Discussion

When comparing CS to monopolar stimulation with high-density electrodes, the neural probability model shows that high-density electrodes are more localized. CS does activate fibers normally not stimulated by a single contemporary electrode, however, inserting a high-density electrode beneath the same fibers creates a more localized spread of excitation. Fig. 6a demonstrates why CS with $\alpha = 0.5$ produces a wider spread of excitation, but stimulates fewer neurons than a high-density electrode. For CS, the AFs for two electrodes are summed, and the resulting AF is almost twice as wide as the AF from a single electrode. The decrease in strength is the result of the weighted current. Due to the electrode spacing, the summed AF of CS is never more than 50%. As a result, CS requires greater current to stimulate the same number of neurons as a single high-density electrode.

With CF, while the spread of excitation generated by the high-density electrodes was narrower, the current required to activate the same number of neurons as the contemporary electrodes was significantly higher. For the contemporary electrodes (Fig. 6b), since the spacing is 1 mm, the side electrodes do not greatly detract from the strength of the center electrode in the summation. However, for the high-

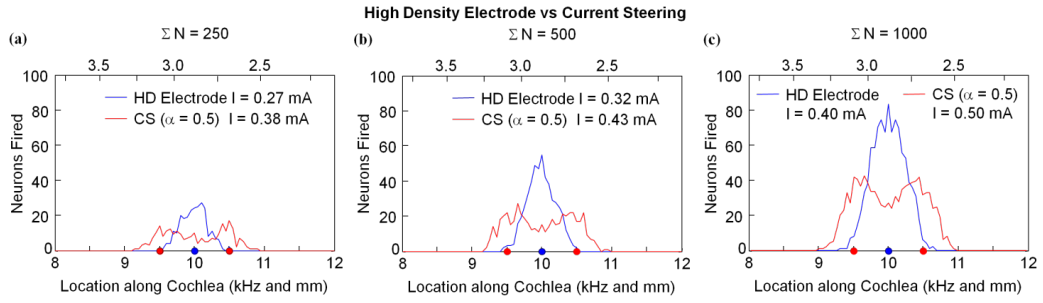

Fig. 4. Comparison of monopolar high-density stimulation to CS: (a) for $\Sigma N = 250$, (b) for $\Sigma N = 500$, (c) for $\Sigma N = 1000$. On the x-axis, frequency is located at the top of the plot and distance is located at the bottom.

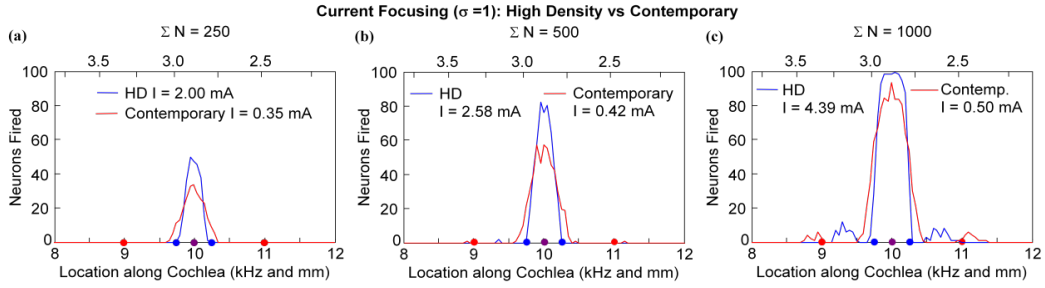

Fig. 5. Comparison of current focusing with $\sigma = 1$ for high-density electrodes and contemporary electrodes: (a) for $\Sigma N = 250$, (b) for $\Sigma N = 500$, (c) for $\Sigma N = 1000$. On the x-axis, frequency is located at the top of the plot and distance is located at the bottom.

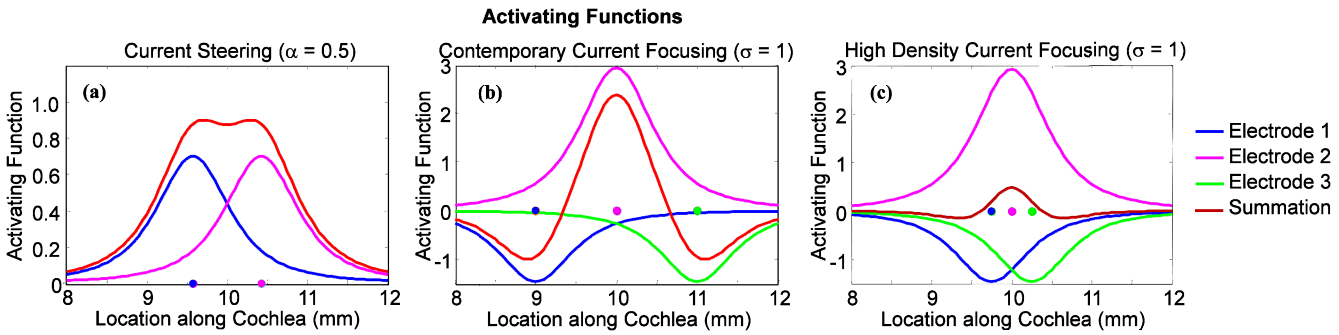

Fig. 6. Activating functions of (a) current steering at α = 0.5, (b) contemporary current focusing at σ = 1, and (c) high-density current focusing at σ = 1.

density electrodes (Fig. 6c), the spacing of 0.25 mm enables the side electrodes to have a much greater impact on the strength of the center electrode in the summation. It is important to note that the side lobes in the activating function play a role in the propagation of the neural signal and it may be advantageous to minimize their respective strength. In summary, this demonstrates a natural tradeoff between focused stimulation and required current.

VI. Conclusion

This first-order estimation model provides a solid foundation for the investigation of high-density electrodes in CIs. The model presented here makes a very fundamental assumption that the neural fibers are organized in a regular fashion with respect to the electrode array. Further evaluations using a second-order estimation model are currently being pursued which incorporate the three-dimensional nature of the auditory nerve. It is likely that the number of neurons fired may not be the measure to validate the efficacy of high-density stimulation, but rather the specificity of neurons fired. Moreover, the model estimates each electrode as a point source. To improve our estimates a dimensionally accurate representation of the electrode array will be developed in a 3D CAD program. In addition, the conductive properties of the scala media of the cochlea will be modeled in a finite element method (FEM) software.

The purpose of this research was to validate the increased performance of high-density stimulating arrays for CIs. The results revealed that sites on high-density electrode arrays provide more precise stimulation using less current than contemporary arrays. This result is particularly relevant because minimizing power consumption and extending battery life for CI users is a priority [20]. Such arrays will likely provide a low-power, high resolution alternative to contemporary electrode arrays employing current steering techniques.

References

[1] B. S. Wilson and M. F. Dorman, "Cochlear implants: Current designs and future possibilities," *Journal of Rehabilitation Research and Development*, vol. 45, no. 5, pp. 696–730, 2008.

[2] B. Bonham and L. Litvak, "Current focusing and steering: Modeling, physiology, and psychophysics," *Hearing Research*, vol. 242, no. 1-2, pp. 141–153, Aug. 2008.

[3] K. D. Wise, P. T. Bhatti, J. Wang, and C. R. Friedrich, "High-density cochlear implants with position sensing and control," *Hearing Research*, vol. 242, pp. 22–30, 2008.

[4] K. Iverson, P. T. Bhatti, J. D. Falcone , and B. R. McKinnon, "Cochlear Implantation using thin-film array electrodes," *Otolaryngology-Head and Neck Surgery Journal*, in press.

[5] "HiFocus Electrode Series," *Advanced Bionics*, http://www.advancedbionics.com.

[6] "Technical Specifications Nucleus® 5 Cochlear Implant (CI512)," *Cochlear Ltd*, http://products.cochlearamericas.com.

[7] "PULSARCI^{100} Technical Specifications" *Med-El,* http://www.cochlearimplants.com/ENG/US/20_Products/10_Cochlear_Implants/999_p_tech.asp.

[8] "Cochlear Implant System, Digisonic SP," *MxM Neurelec,* http://www.neurelec.com.

[9] J. B. Firszt, D. B. Koch, M. Downing, and L. Litvak, "Current steering creates additional pitch percepts in adult cochlear implant recipients," *Otology and Neurotology*, vol. 28, pp. 629–636, 2007.

[10] Advanced Bionics©, "HiRes with FideltyTM 120 Sound Processing," [White Paper] *Boston Scientific*, Sept. 2006.

[11] C. K. Berenstein, L. H. M. Mens, J. J. S. Mulderr, and F. J. Vanpouke, "Current steering and current focusing in cochlear implants: Comparison of monopolar, tripolar and virtual channel electrode configurations," *Ear & Hearing*, vol. 29, no. 2, pp. 250–260, 2008.

[12] F. Rattay, "Analysis of models for external stimulation of axons," *IEEE Transactions on Biomedical Engineering*, vol. 33, no. 10, pp. 974–977, Oct. 1986.

[13] L. Tung, "Chapter 2.3: The generalized activating function", *Cardiac Bioelectric Therapy: Mechanisms and Practical Implications*, 1st ed. vol. 1, I. R. Efimov, M. W. Kroll, and P. J. Tchou (Eds.), New York: Springer Science + Business Media, LLC, 2009, pp. 125–132.

[14] C. T. M. Choi and C. Hsu, "Conditions for Generating Virtual Channels in Cochlear Prosthesis Systems," *Annals of Biomedical Engineering*, vol. 37, no. 3, pp. 614–624, Mar. 2009.

[15] L. M. Litvak, A. J. Spahr, and G. Emadi, "Loudness growth observed under partially tripolar stimulation: Model and data from cochlear implant listeners," *Journal of Acoustical Society of America*, vol. 122, no. 2, pp. 967–981, Aug. 2007.

[16] Y. Xu and L. M. Collins, "Threshold prediction for noise-modulated electrical stimuli using a stochastic auditory nerve model: Implications for cochlear implants," *IEEE International Conference on Acoustics, Speech and Signal Processing - Proceedings*, vol. 2, pp. II/1929–II/1932, 2002.

[17] D. Greenwood, "A cochlear frequency-position function for several species – 29 years later," *Journal of Acoustical Society of America*, vol. 87, no. 6, pp. 2592–2605, June 1990.

[18] O. Stakhovskaya, D. Sridhar, B. H. Bonham, and P. A. Leake, "Frequency map for the human cochlear spiral ganglion: implications for cochlear implants," *Journal of the Association for Research in Otolaryngology*, vol. 8, no. 2, pp. 220–233, June 2007.

[19] J. Frijns, R. Kalkman, F. Vanpoucke, J. Bongers, and J. Briare, "Simultaneous and non-simultaneous dual electrode stimulation in cochlear implants: evidence for two neural response modalities," *Acta Oto-Larngologica*, vol. 129, pp. 433–439, 2009.

[20] F.-G. Zeng, S. Rebscher, W. Harrison, X. Sun, and H. Feng, "Cochlear Implants: System Design, Integration, and Evaluation," *IEEE Reviews in Biomedical Engineering*, vol. 1, pp. 115–142, 2008.